

## A Photoionization model for the Infrared Coronal Line Emission in the Classical Nova V1716 Scorpii

C. E. WOODWARD<sup>†</sup> <sup>1</sup>, G. SHAW <sup>2</sup>, S. STARRFIELD <sup>3</sup>, A. EVANS <sup>4</sup> AND K. L. PAGE <sup>5</sup>

<sup>1</sup>Minnesota Institute for Astrophysics, University of Minnesota, 116 Church Street SE, Minneapolis, MN 55455, USA

<sup>2</sup>Department of Astronomy and Astrophysics, Tata Institute of Fundamental Research, Homi Bhabha Road, Mumbai 400005, India

<sup>3</sup>School of Earth & Space Exploration, Arizona State University, Box 876004, Tempe, AZ 85287-6004, USA

<sup>4</sup>Astrophysics Group, Keele University, Keele, Staffordshire, ST5 5BG, UK

<sup>5</sup>School of Physics & Astronomy, University of Leicester, Leicester, LE1 7RH, UK

(Received 2023 Nov 09; Accepted 2024 Apr 17; Published To appear in the Astrophysical J.)

### ABSTRACT

A near-infrared spectrum of nova V1716 Scorpii (PNV J17224490-4137160), a recent bright ( $V_{max} = 7.3$  mag), Fermi-LAT detected  $\gamma$ -ray source, was modeled using the photoionization code CLOUDY. Abundances were estimated for He, C, N, O, Si, Al, Mg, Fe, Ne, S, Ca, and P. Notably, P (a factor of 120) and N (a factor of 248) are highly overabundant. It was necessary to assume the ejecta consist of two components (with a cylindrical geometry): a dense component from which the bulk of the H, He, and neutral O I and N emission arises and a more diffuse component from which most of the coronal lines arise. Some of the coronal lines are found to originate from both the dense and diffuse components. The mass of the ejecta, including neutral and ionized gas, is  $\simeq 4.19 \times 10^{-4} M_{\odot}$ . Our analysis indicates that in the case of V1716 Sco (which has a carbon-oxygen white dwarf), a fraction of 25% white dwarf matter rather than 50% is favored for the mixing between white dwarf and the accreted envelope before the outburst. This mixing ratio is like that found for Oxygen-Neon novae where a 25% mixing fraction is also indicated. Helium hydride – the first molecule to form after the Big Bang – may have formed in the ejecta of V1716 Sco based on photoionization modeling. This prediction suggests that novae may be potential formation sites of this important molecular ion.

**Keywords:** Fast novae (530), Chemical abundances (224), Chemical enrichment (225), Explosive Nucleosynthesis (503), Theoretical models (2107)

### 1. INTRODUCTION

Classical nova (CN) explosions occur in semi-detached binary systems consisting of a white dwarf (WD) component and a main sequence dwarf. The latter fills its Roche Lobe, and consequently material spills on to the surface of the WD via an accretion disk. In time the material at the base of the accreted layer becomes degenerate, and hot enough to trigger a thermonuclear runaway (TNR). This results in a CN explosion, and the ejection of  $\simeq 10^{-5}$  to  $10^{-4} M_{\odot}$  of material, enriched in C, N, O, Mg, Si, Al, Ne, and other metals,

at several 100 to  $\gtrsim 1000 \text{ km s}^{-1}$  (e.g., Bode & Evans 2012; Anupama & Kamath 2012). In view of the Galactic CN rate ( $\simeq 47 \text{ yr}^{-1}$ ; De et al. 2021), likely CNe are a major source of  $^{13}\text{C}$ ,  $^{15}\text{N}$  and  $^{17}\text{O}$  in the Galaxy (Gehrz et al. 1998; Bode & Evans 2012) and may make a significant contribution to Galactic  $^7\text{Li}$  (Starrfield et al. 2020, 2024), although the case for this rests on observational results and not theory (José et al. 2020; Kemp et al. 2022; Molaro et al. 2022, 2023).

As the ejecta disperse, an emission line spectrum is produced and stable nuclear burning causes the pseudophotosphere to shrink, revealing a hotter, deeper source of emission. CNe spectra are remarkable for their changing elemental and ion content and the temporal development of line profiles is critical to understanding the dynamics of ejection. Low-energy permitted lines of CNO and Fe II give way to He II, as well as high ionization lines, e.g., [Fe VII] 6087 Å, and ultimately to infrared (IR) “coronal” lines (Raj et al. 2015;

Corresponding author: C.E. Woodward  
mailto:chickw024@gmail.com

<sup>†</sup> Visiting Astronomer at the Infrared Telescope Facility, which is operated by the University of Hawaii under contract 80HQTR19D0030 with the National Aeronautics and Space Administration.

Woodward et al. 2021; Kumar et al. 2022). The latter lines are sources of abundance information as a wide range of iso-electronic sequences (Greenhouse et al. 1990) and adjacent ionization states of metals are observable. Often, as the ejecta cool and evolve, molecules (e.g., CO – Rudy et al. 2003; Pontefract & Rawlings 2004; Das et al. 2009; Banerjee et al. 2016) and dust form. CNe originating on CO WDs are often dust-formers and, while C is a major grain component, silicates, polycyclic aromatic hydrocarbons (PAHs), and SiC are often present, occasionally in the same nova (Evans & Gehrz 2012).

The evolution of the TNR depends upon the mass and luminosity of the WD, the rate of mass accretion, the composition of the accreted material, and the chemical composition in the reacting layers. Hydrodynamic studies of the accretion process on to the WD preceding the TNR event and the degree to which material from the underlying WD and the envelope is admixed in the ejecta has been studied by many groups for several decades (Politano et al. 1995; Glasner et al. 2012; Kelly et al. 2013; José et al. 2020; Starrfield et al. 2020, 2024). However, the constraints on the theoretical models of nucleosynthesis in the outburst, chemical anomalies related to nucleosynthesis, and the evolution of the progenitor are provided by spectroscopic observations of the ejecta from which detailed elemental abundance patterns can be derived.

In this paper we estimate ejecta abundances for V1716 Sco in the coronal line phase of its evolution 132.8 days after outburst (Woodward et al. 2023) derived from photoionization modeling of IR (0.7 to 4.2  $\mu\text{m}$ ) spectra using CLOUDY (Ferland et al. 1998; Chatzikos et al. 2023). These abundance patterns are compared with theoretical simulations of CNe (Starrfield et al. 2020, 2024) with differing core-envelope mixing ratios and their ejecta abundance patterns to understand the characteristics of the underlying WD. Since the coronal phase is fairly prevalent in novae (e.g., the statistics compiled by Benjamin & Dinerstein 1990), the present work may serve as a useful template for comparing results from similar near-IR modeling of CNe that may erupt in the future.

## 2. V1716 SCO

### 2.1. General Properties

Nova V1716 Sco (PNV J17224490-4137160) was discovered on 2023 April 20.6780 UT by A. Pearce.<sup>1</sup> The nova was bright on 2023 April 20.410 UT (MJD 60054.410; Sokolovsky et al. 2023), which we take as our origin of time ( $t_0$ ). Its CN status was confirmed by Walter & Pearce (2023), who described it as a lightly-reddened Fe II nova near maximum light. Optical spectroscopy of the earliest phases was obtained by Shore et al. (2023a,b,c) and

Izzo et al. (2023). The early optical spectra showed ejection velocities  $\simeq 1700 \text{ km s}^{-1}$ , although there were emission components extending to  $\pm 3000 \text{ km s}^{-1}$ . The Neil Gehrels Swift Observatory (Gehrels et al. 2004) has observed V1716 Sco regularly since outburst; details will be presented elsewhere. NuSTAR observations of the hard X-ray spectrum of V1716 Sco early in the outburst (Sokolovsky et al. 2023) revealed a heavily absorbed thermal plasma. V1716 Sco joins the increasing inventory of CNe that are  $\gamma$ -ray sources (Cheung et al. 2015, 2018).

V1716 Sco is a fast nova (for speed-class definition, see Chomiuk et al. 2021). The AAVSO V-band light curve yields  $t_2$  and  $t_3$  values ( $t_2$  and  $t_3$  are the times to decline by 2 and 3 magnitudes respectively from peak brightness) of  $\sim 5.8$  and 11.7 d respectively.

### 2.2. Distance and Reddening

The reddening,  $E_{B-V}$ , to V1716 Sco was estimated by Shore et al. (2023b) to be in the range  $0.45 \lesssim E_{B-V} \lesssim 0.6$ , consistent with the lower limit ( $E_{B-V} \gtrsim 0.5$  from diffuse interstellar absorption features) given by Izzo et al. (2023). The methods of van den Bergh & Younger (1987) using the intrinsic colors of CNe give  $E_{B-V} = 0.66$  (color at maximum light) and  $E_{B-V} = 0.70$  (color at time  $t_2$ ). Using the simultaneous solution for  $A_V$  and distance,  $D$ , method described in Kumar et al. (2022), we obtain  $D = 3.6 \pm 0.6 \text{ kpc}$  and a somewhat higher value of reddening,  $E_{B-V} = 1.0$ . The relative strengths of the OI 0.8446 and 1.1287  $\mu\text{m}$  lines can be used to estimate the reddening to the nova (Srivastava et al. 2016). Their ratio, as obtained from the spectrum presented here, suggests  $E_{B-V} \sim 0.57$  using a Cardelli et al. (1989) interstellar extinction law. For the present work it seems reasonable to adopt a value of  $E_{B-V} = 0.65$  (the average of all estimates is  $0.64 \pm 0.18$ ).

For a value of  $E_{B-V} = 0.65$ , the distance,  $D$ , is found to be  $\sim 2.1 \text{ kpc}$  from the extinction versus distance relation derived by Marshall et al. (2006). A 19<sup>th</sup> magnitude star (Gaia DR3 5959616875349110656) is found to closely match the position of V1716 Sco (the offset between this star and the nova is  $0''.42$ ). This star has a parallax of 1.0863 mas and parallax error of 0.3907 mas in the EDR3 database (Gaia Collaboration et al. 2023). A search of the Dark Energy Camera Plane Survey (DECaPS, Saydjari et al. 2023) using a  $2''$  cone search around the position of V1716 Sco with the Astro Data Lab query interface (Nikutta et al. 2020) and the DECaPS DR2 did not return any cataloged points sources. We assume that the Gaia positionally associated source is the progenitor

<sup>1</sup> <http://www.cbat.eps.harvard.edu/unconf/followups/J17224490-4137160.html>

star of the nova. As recommended for the Gaia data, when the fractional parallax uncertainties are not too large (as applicable in this case) use of the Gaia geometric distance ( $3.17^{+2.2}_{-1.6}$  kpc) is suggested rather than that of the Gaia photogeometric distance, which in this case is  $4.97^{+1.7}_{-1.1}$  kpc (Bailer-Jones et al. 2021). Thus for the present work we adopt  $D \simeq 3$  kpc (a value close to the Gaia geometric distance), although there is considerable uncertainty.

### 3. OBSERVATIONS

A 0.7 to 4.2  $\mu\text{m}$  spectrum of V1716 Sco was obtained on 2023 August 31.24 UT (MJD 60187.24) on the 3.2 m NASA Infrared Telescope Facility (IRTF). Observations were obtained with the medium-resolution facility spectrograph (SpeX, Rayner et al. 2003) in the cross-dispersed short (SXD) and long (LXD\_short) modes to cover the spectral range of 0.7 - 4.2  $\mu\text{m}$ . The observations were made with a  $0''.5$  slit ( $R = 1200$ ), at an airmass between 2.10 - 2.24, under photometric conditions and moderate seeing ( $\lesssim 1''.1$  in the K-band). The A0V star HD 148418 was used to correct for telluric absorption and the total on-source integration times for V1716 Sco were 1978s and 556s respectively (the SXD and LXD modes). The SpeX data were reduced and calibrated using Spextool (Cushing et al. 2004) and the tool xtellcor (Vacca et al. 2003) was used for the corrections for telluric absorption. The observed spectrum is presented in Figure 1.

The Swift soft X-ray spectrum of 31 August 2023 (MJD 60187.33083  $\pm$  0.00627; obtained within 2 hrs of the IR spectrum) was parametrized by a blackbody and provided an initial estimate for  $T_{\text{BB}}(\text{K})$ . The spectrum is shown in Figure 2 fitted by a BB with  $kT = 23.6^{+3.1}_{-3.6}$  eV, or  $\log T (\text{K}) = 5.44$ . As an initial estimate for the bolometric luminosity  $L_{\text{bol}}$ , the BVRI data at maximum from AAVSO were dereddened and fitted by a blackbody to give a temperature of  $\sim 8400$  K equivalent to an outburst luminosity  $\simeq 10^{38.45}$  ergs  $\text{s}^{-1}$  for a distance of 3 kpc. The latter BB has a radius of  $8.9 \times 10^{12}$  cm (adopting an expansion velocity of 1000 km  $\text{s}^{-1}$  and  $t = 130\text{d}$ ).

V1716 Sco entered a super-soft x-ray (SSS) phase near day 55 (Page & Kuin 2023). Spectral fits (assuming a simple BB for the SSS source) to all the Swift x-ray spectra suggest only a slight increase in the temperature ( $\simeq 30$  eV) between day 133 and 180 but nothing significant, as shown in Figure 3.

## 4. RESULTS

### 4.1. Photoionization Models

#### 4.1.1. Photoionization Models - Cylindrical Geometry

The photoionization spectral synthesis code CLOUDY (version C23.01 Chatzikos et al. 2023) was used to model the IR spectroscopic data of V1716 Sco. We assume the sur-

**Table 1.** V1716 Sco CLOUDY Parameters

Cylindrical	Day
Model	+132.8
$\log T_{\text{BB}}(\text{K})$	5.74
$\log L(\text{erg s}^{-1})$	37.5
$\log H_{\text{den}}(\text{LD - diffuse})(\text{cm}^{-3})$	6.40
$\log H_{\text{den}}(\text{HD - clump})(\text{cm}^{-3})$	7.85
$\log R_{\text{in}}(\text{cm})$	15.01
$\log R_{\text{out}}(\text{cm})$	15.3367
$\log h (\text{cm})$	15.35
Covering factor	0.5
Filling factor (diffuse)	0.80
Filling factor (clump)	0.20
<u>Abundances</u> <sup>a)</sup>	
He/H	$18.72 \times 10^{-2}$
C/H	$17.41 \times 10^{-4}$
N/H	$167.65 \times 10^{-4}$
O/H	$93.09 \times 10^{-4}$
Ne/H	$2.18 \times 10^{-4}$
S/H	$98.99 \times 10^{-6}$
Si/H	$71.28 \times 10^{-6}$
Al/H	$16.92 \times 10^{-6}$
Mg/H	$11.94 \times 10^{-5}$
Ca/H	$5.26 \times 10^{-6}$
P/H	$30.84 \times 10^{-6}$
Fe/H	$63.20 \times 10^{-6}$
Total number of lines	39
Number of free parameters	16
Degrees of freedom	23
Reduced $\chi^2$	2

<sup>a)</sup>Cloudy23.01 model abundances are optimized assuming the abundances given in Grevesse et al. (2010).

NOTE—All other elements have non-depleted (with respect to H) solar abundances.

face of the central WD is emitting ionizing blackbody radiation with a temperature  $T_{\text{BB}}(\text{K})$  and a bolometric luminosity,  $L_{\text{bol}}$  (erg  $\text{s}^{-1}$ ), irradiating a cylindrical geometry of gas expanding with a velocity of  $v_{\text{exp}}$  (km  $\text{s}^{-1}$ ). The cylindrical model in CLOUDY is basically a truncated spherical model. The dimension of this gas is defined by an inner radius  $r_{\text{in}}$  (cm), thickness  $r_{\text{d}}$  (cm), and the height of the cylinder  $h$  (cm). CNe often exhibit asymmetric geometries that are highly non-spherical, containing knots and clumps of mate-

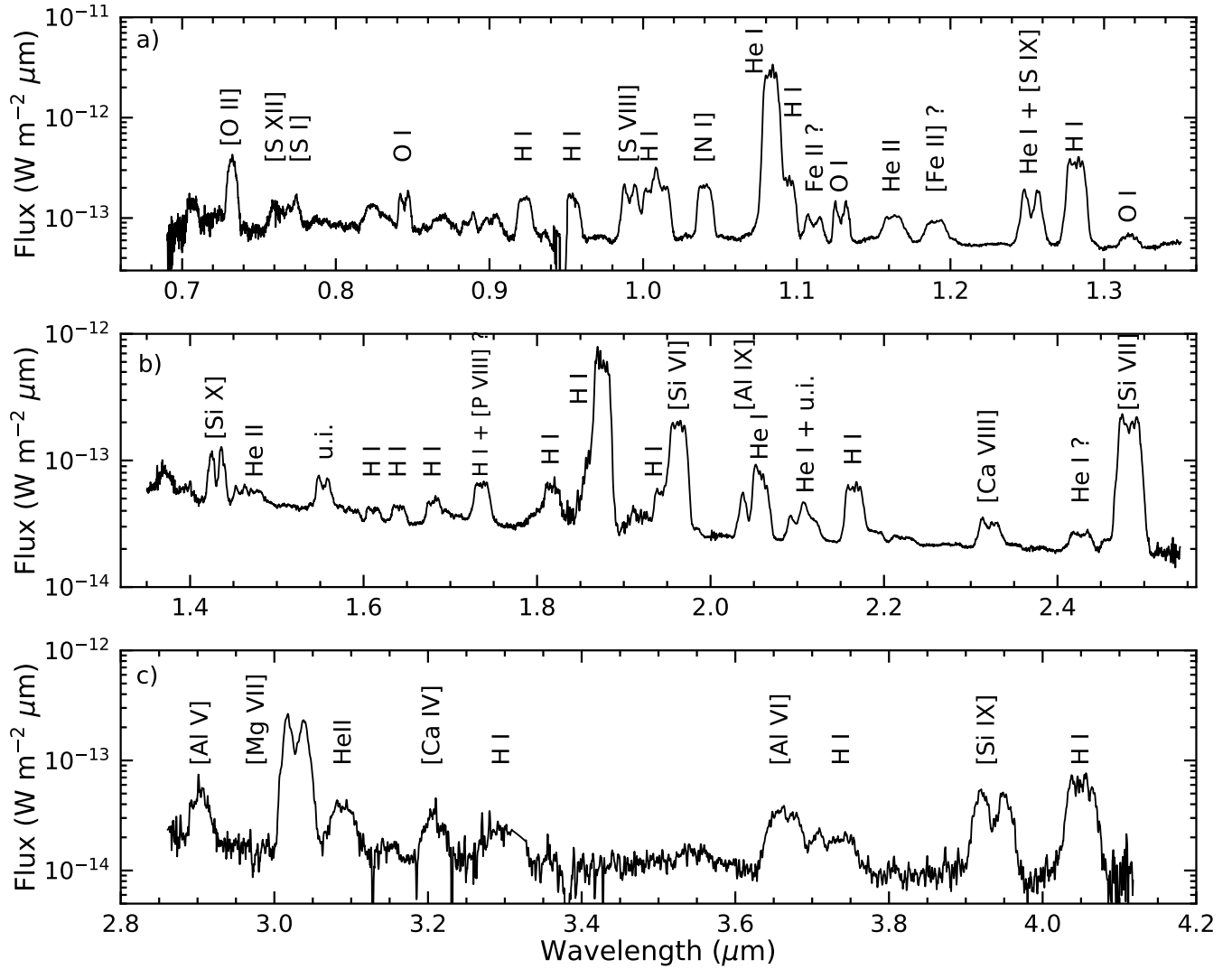


**Figure 1.** The observed spectrum of V1716 Sco on day +132.8, with the prominent lines identified. a) the 0.66 to 1.34  $\mu\text{m}$  section (SpeX SXD). b) the 1.35 to 2.5  $\mu\text{m}$  section (SpeX SXD), and c) the 2.80 to 4.20  $\mu\text{m}$  section. For these latter data, the observed spectral segment (SpeX LX) was smoothed with a Savitsky-Golay filter of window width = 7, polynomial order = 2, to improve the SNR and each end of the spectral segments were clipped (where the SNR  $\lesssim 3$ ). Unidentified lines are indicated with 'u.i.'. The observed spectrum (DbF) for each panel is available as a machine readable table (MRT) in the on-line manuscript.

rial (for example V1280 Sco, T Pydixis, or RR Pic, Chesneau et al. 2012; Toraskar et al. 2013; Celedón et al. 2024) motivating use of a cylindrical model. The solar abundances called in the Cloudy modeling are from Grevesse et al. (2010).

In the model presented here, we assume a number density law proportional to  $n_{\text{in}}r^{-3}$ , where  $n_{\text{in}}(\text{cm}^{-3})$  is the total hydrogen number density,

$$n_{\text{in}}(\text{H}^0) + n_{\text{in}}(\text{H}^+) + 2 \times n_{\text{in}}(\text{H}_2) + \sum_{\text{other}} n_{\text{in}}(\text{H}_{\text{other}}), \quad (1)$$

the latter term being the summation of other species containing hydrogen nuclei such as  $\text{H}_3^+$ ,  $\text{H}_2^+$ , etc. The observed  $v_{\text{exp}}$  ranges over 1000 to 1350  $\text{km s}^{-1}$ . We adopt  $v_{\text{exp}} = 1000 \text{ km s}^{-1}$ . Hence, both  $r_{\text{in}}$  (cm) and  $r_{\text{d}}$  (cm) are

set by observation. However, the cylindrical height is a free parameter. The physical parameters and their values for our final “best-fit” model are listed in Table 1. Later, we consider the observed velocity range as well as an additional model variable.

The observed spectrum exhibits highly ionized lines (Si X, Si IX) and neutral lines (H I, O I, He I). The physical processes of forming these lines differ. In the default mode, CLOUDY considers both photoionization and collisional ionization. The collisional ionization rate coefficients are from Voronov (1997) and Dere (2007). In the current model both photoionization and collisional ionization processes are enabled, so strictly it is not a pure photoionization model. However, most of the lines are generated through

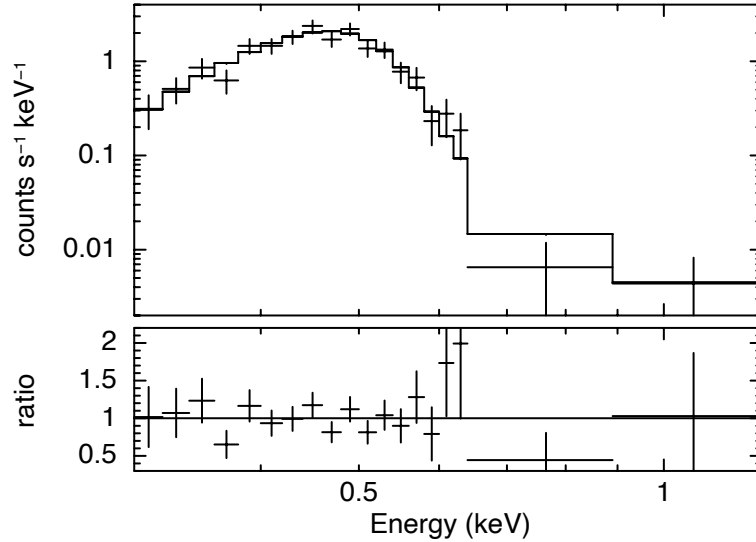


**Figure 2.** The Swift x-ray spectrum of V1716 Sco obtained contemporaneously with the near-IR spectrum. The top panel shows a blackbody fit using HEASOFT XSPEC tools (Arnaud 1996) to the soft emission with  $kT = 23.6^{+3.1}_{-3.6}$  eV (or  $\log(T) = 5.44$  K). The bottom panel is the ratio of the data to the model fit.

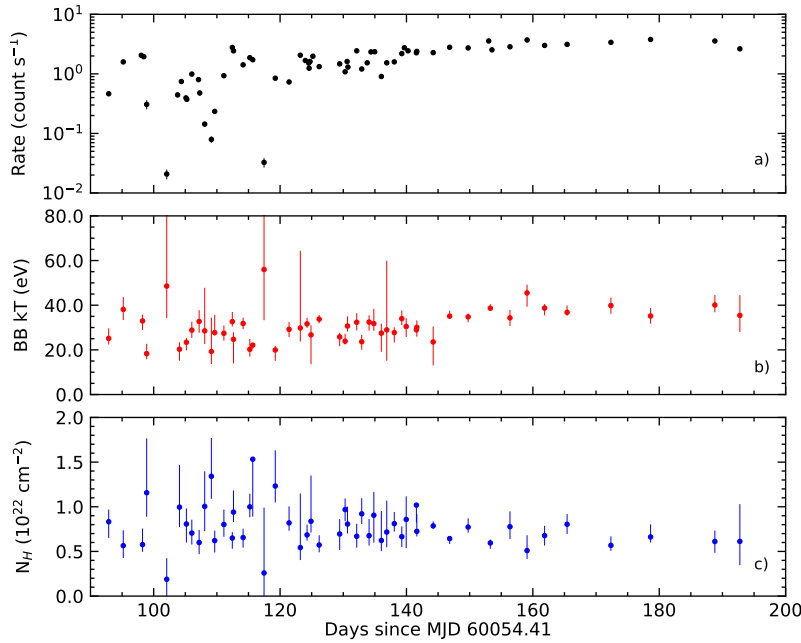


**Figure 3.** Synoptic Swift observations of V1716 Sco post outburst and spectral fits. a) The light curve. b) The derived  $kT$  (eV) from model fits assuming a simple blackbody for the SSS for the soft x-ray spectra (red points with associated asymmetric error). Only a modest variance in the overall temperature of the x-ray source from day 133 through day 190 is evident. c) The derived hydrogen column density (blue dots with associated asymmetric errors). The data for each panel are available as a machine readable table (MRT) in the on-line manuscript.

photoionization and recombination. CLOUDY has options to use these processes separately. However, for V1716 Sco, the combined photoionization and collisional model works better (as compared to the observations) than a solely collisional or solely photoionization model.

We assume a two component model, consisting of high (“clump”) and low densities (“diffuse”). The highly ionized lines arise from the low density component (A), whereas the neutral lines arise from the high density component (B). While the density and the filling factors for these two com-



ponents are different, the other modeling parameters are the same. Our final model predicts an average hydrogen density at the inner radius,  $r_{\text{in}}$  for components A and B to be  $\log H_{\text{den}} (\text{cm}^{-3}) = 6.4$  and  $7.85$ , respectively. Component A and component B contain 12% and 88% of the volume of the ejecta, respectively. In component B, a density higher than  $\log H_{\text{den}} = 7.85$  reduces the forbidden line fluxes due to increased collisional de-excitations.

We find that a blackbody of temperature  $10^{5.74}$  K with bolometric luminosity  $10^{37.5}$   $\text{erg s}^{-1}$  is required to reproduce the observed line intensities on day 133. This high blackbody temperature is necessary to reproduce highly ionized line fluxes, such as for Si IX. On the other hand, a luminosity of  $10^{37.5}$   $\text{erg s}^{-1}$  makes the forbidden lines much weaker and the H I lines much stronger than is observed. The physical parameters and their values for the cylindrical model best-fit are listed in Table 1. We vary only the elemental abundances of the observed lines (He, O, N, Mg, P, Ca, Al, S, Si). Most of the predicted line intensities match with their observed values within the observed uncertainties (see Table 2).

#### 4.1.2. Photoionization Models - Spherical Geometry

As a check, we consider a spherical geometry of the ejecta. In Table 3, we present our predictions for the spherical model keeping all the input parameters the same as the cylindrical model. Our model predictions with a cylindrical geometry match better with the observations despite the cylindrical model being a very simple truncated spherical model (see Fig. 4). Hence, we consider the cylindrical model as our best fit model.

#### 4.1.3. Photoionization Models - Ejecta Velocity

Observation reveals that  $v_{\text{exp}}$  ranges from 1000 - 1350  $\text{km s}^{-1}$ , i.e., close to half the FWHM of the hydrogen Paschen- $\beta$  line of 2700  $\text{km s}^{-1}$ . Generally the  $v_{\text{exp}}$  is typically half the FWHM for any expanding spherical shell of gas (Robinson et al. 1982). Hence, for the cylindrical model, we assume the low density component expanding at 1350  $\text{km s}^{-1}$  which is greater than the expansion velocity of the dense component. The results are listed in Table 4. This model increases the [Si X] line flux by 0.05 dex. Considering all the three cases mentioned above, (see Fig. 4), a cylindrical model with low density region expanding with a higher velocity than the high density region seems to be the best fit model.

#### 4.1.4. Photoionization Models - Goodness of Fit

The  $\chi^2$ , the goodness of fit of a model to the observed spectrum, is determined by the following relation,

$$\chi^2 = \sum_{i=1}^n \frac{(M_i - O_i)^2}{\sigma_i^2} \quad (2)$$

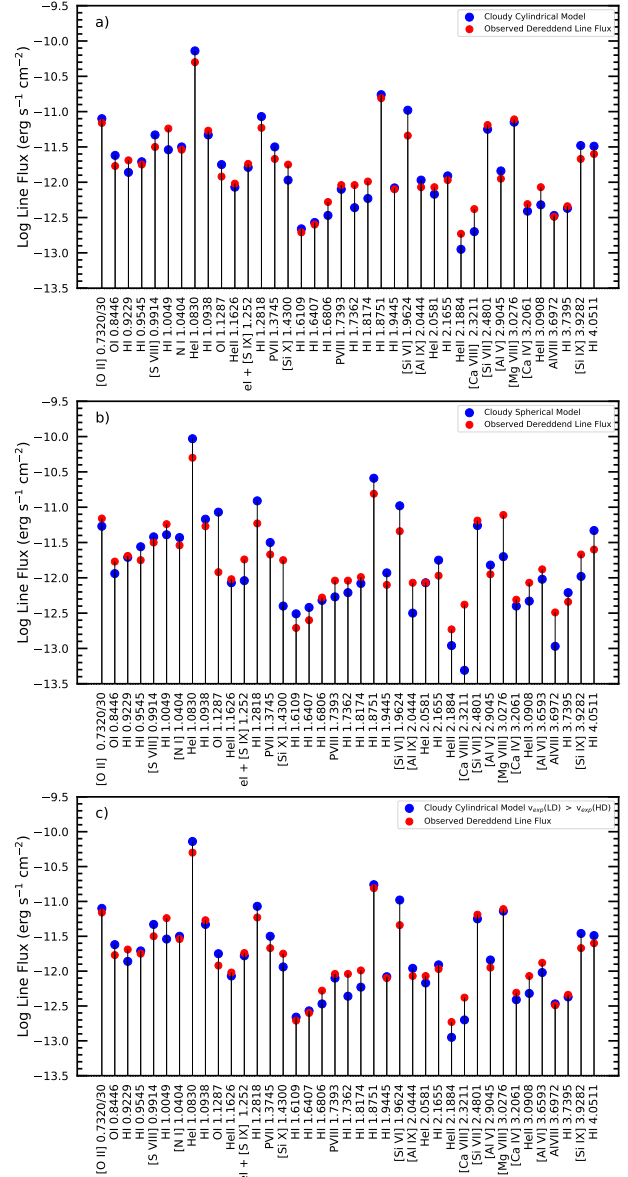


**Figure 4.** Observed dereddened line fluxes (red filled circles) versus CLOUDY line fluxes (blue filled circles). a) From the best-fit cylindrical model (Table 2). b) From a spherical model (Table 3). c) From the best-fit cylindrical model (Table 4) where the LD component is expanding with a velocity greater than the HD component.

where  $n$  is the number of emission lines used in the model,  $M_i$  and  $O_i$  are the modeled and observed line flux ratios (line fluxes were normalized with respect to the Paschen- $\beta$  line), and  $\sigma_i$  is the error in the observed line flux ratios. The reduced  $\chi^2$  (reported in Table 1) is given by  $\chi_{\text{red}}^2 = \chi^2/\nu$ , where  $\nu$  is the number of degrees of freedom, given by the difference between the number of observed emission lines ( $n$ ) and the number of free parameters ( $n_p$ ), where  $\nu = n - n_p$ . For acceptable fitting, the value of  $\chi^2 \sim \nu$  and  $\chi_{\text{red}}^2$  should be low, typically between 1 and 2. The value of  $\sigma$  gen-

**Table 2.** V1716 Sco Observed and CLOUDY Line Luminosities for the Cylindrical Model

Line	log flux <sup>†</sup> (LD)	log flux <sup>†</sup> (HD)	log total flux (HD + LD)	Dereddend Observed Flux
( $\mu\text{m}$ )	( $\text{erg s}^{-1} \text{cm}^{-2}$ )	( $\text{erg s}^{-1} \text{cm}^{-2}$ )	( $\text{erg s}^{-1} \text{cm}^{-2}$ )	( $\text{erg s}^{-1} \text{cm}^{-2}$ )
[O II] 0.7320/30	-20.13	-11.10	-11.10	-11.16
O I 0.8446	<-20.00	-11.62	-11.62	-11.77
HI 0.9229	-13.96	-11.86	-11.86	-11.69
HI 0.9545	-13.80	-11.72	-11.71	-11.75
[S VIII] 0.9914	-11.91	-11.47	-11.33	-11.50
HI 1.0049	-13.62	-11.54	-11.54	-11.24
[N I] 1.0404	<-20.00	-11.50	-11.50	-11.54
He I 1.0830	-14.99	-10.14	-10.14	-10.30
HI 1.0938	-13.42	-11.33	-11.33	-11.27
O I 1.1287	<-20.00	-11.75	-11.75	-11.92
He II 1.1626	-13.39	-12.09	-12.07	-12.02
He I + [S IX] 1.252	-11.93	-12.36	-11.79	-11.74
HI 1.2818	-13.13	-11.07	-11.07	-11.23
P VII 1.3745	-13.43	-11.50	-11.50	-11.67
[Si X] 1.4300	-11.99	-16.21	-11.97	-11.75
HI 1.6109	-14.81	-12.66	-12.66	-12.71
HI 1.6407	-14.70	-12.57	-12.57	-12.60
HI 1.6806	-14.58	-12.47	-12.47	-12.28
P VIII 1.7393	-12.47	-12.35	-12.10	-12.04
HI 1.7362	-14.47	-12.36	-12.36	-12.04
HI 1.8174	-14.33	-12.23	-12.23	-11.99
HI 1.8751	-12.86	-10.76	-10.76	-10.81
HI 1.9445	-14.17	-12.08	-12.08	-12.10
[Si VI] 1.9624	-14.50	-10.98	-10.98	-11.34
[Al IX] 2.0444	-11.97	-14.48	-11.97	-12.07
He I 2.0581	-19.04	-12.17	-12.17	-12.07
HI 2.1655	-13.99	-11.91	-11.91	-11.97
He II 2.1884	-14.26	-12.97	-12.95	-12.73
[Ca VIII] 2.3211	-12.71	-14.47	-12.70	-12.38
[Si VII] 2.4801	-12.59	-11.27	-11.25	-11.19
[Al V] 2.9045	-17.24	-11.84	-11.84	-11.95
[Mg VIII] 3.0276	-11.16	-13.02	-11.15	-11.11
[Ca IV] 3.2061	-18.70	-12.41	-12.41	-12.31
He II 3.0908	-13.66	-12.34	-12.32	-12.07
[Al VI] 3.6593	-14.28	-12.02	-12.02	-11.88
Al VIII 3.6972	-12.50	-13.72	-12.47	-12.49
HI 3.7395	-14.46	-12.37	-12.37,	-12.34
[Si IX] 3.9282	-11.48	-14.96	-11.48	-11.67
HI 4.0511	-13.55	-11.50	-11.49	-11.60

NOTE—<sup>†</sup> LD/HD = low/high density.

**Table 3.** V1716 Sco Observed and CLOUDY Line Luminosities for the Spherical Model<sup>‡</sup>

Line ( $\mu\text{m}$ )	log flux <sup>†</sup>	log flux <sup>†</sup>	log total flux	Dereddend
	(LD) ( $\text{erg s}^{-1} \text{cm}^{-2}$ )	(HD) ( $\text{erg s}^{-1} \text{cm}^{-2}$ )	(HD + LD) ( $\text{erg s}^{-1} \text{cm}^{-2}$ )	Observed Flux ( $\text{erg s}^{-1} \text{cm}^{-2}$ )
[O II] 0.7320/30	-20.60	-11.27	-11.27	-11.16
O I 0.8446	<-20.00	-11.94	-11.94	-11.77
H I 0.9229	-14.52	-11.71	-11.71	-11.69
H I 0.9545	-14.36	-11.56	-11.56	-11.75
[S VIII] 0.9914	-12.48	-11.46	-11.42	-11.50
H I 1.0049	-14.18	-11.39	-11.39	-11.24
[N I] 1.0404	<-20.00	-11.43	-11.43	-11.54
He I 1.0830	-15.37	-10.03	-10.03	-10.30
H I 1.0938	-13.97	-11.17	-11.17	-11.27
O I 1.1287	<-20.00	-11.07	-11.07	-11.92
He II 1.1626	-13.95	-12.09	-12.07	-12.02
He I + [S IX] 1.252	-12.45	-12.25	-12.04	-11.74
H I 1.2818	-13.65	-10.91	-10.91	-11.23
P VII 1.3745	-14.02	-11.50	-11.50	-11.67
[Si X] 1.4300	-12.40	-16.20	-12.40	-11.75
H I 1.6109	-15.36	-12.51	-12.51	-12.71
H I 1.6407	-15.25	-12.42	-12.42	-12.60
H I 1.6806	-15.14	-12.32	-12.32	-12.28
P VIII 1.7393	-13.04	-12.35	-12.27	-12.04
H I 1.7362	-15.02	-12.21	-12.21	-12.04
H I 1.8174	-14.88	-12.08	-12.08	-11.99
H I 1.8751	-13.38	-10.59	-10.59	-10.81
H I 1.9445	-14.72	-11.93	-11.93	-12.10
[Si VI] 1.9624	-15.09	-10.98	-10.98	-11.34
[Al IX] 2.0444	-12.50	-14.48	-12.50	-12.07
He I 2.0581	-19.50	-12.07	-12.07	-12.07
H I 2.1655	-14.54	-11.76	-11.75	-11.97
He II 2.1884	-14.82	-12.97	-12.96	-12.73
[Ca VIII] 2.3211	-13.34	-14.47	-13.31	-12.38
[Si VII] 2.4801	-13.16	-11.26	-11.26	-11.19
[Al V] 2.9045	-17.84	-11.82	-11.82	-11.95
[Mg VIII] 3.0276	-11.72	-13.02	-11.70	-11.11
[Ca IV] 3.2061	-19.36	-12.40	-12.40	-12.31
He II 3.0908	-14.22	-12.34	-12.33	-12.07
[Al VI] 3.6593	-14.88	-12.02	-12.02	-11.88
Al VIII 3.6972	-13.06	-13.72	-12.97	-12.49
H I 3.7395	-15.00	-12.21	-12.21	-12.34
[Si IX] 3.9282	-11.98	-14.95	-11.98	-11.67
H I 4.0511	-14.08	-11.33	-11.33	-11.60

NOTE—

<sup>‡</sup> All Cloudy input parameters are identical to the cylindrical model.<sup>†</sup> LD/HD = low/high density.



**Table 4.** V1716 Sco Observed and CLOUDY Line Luminosities for the Cylindrical Model where LD is expanding with a higher velocity than the HD

Line ( $\mu\text{m}$ )	log flux <sup>†</sup>	log flux <sup>†</sup>	log total flux	Dereddend
	(LD) ( $\text{erg s}^{-1} \text{cm}^{-2}$ )	(HD) ( $\text{erg s}^{-1} \text{cm}^{-2}$ )	(HD + LD) ( $\text{erg s}^{-1} \text{cm}^{-2}$ )	Observed Flux ( $\text{erg s}^{-1} \text{cm}^{-2}$ )
[O II] 0.7320/30	-20.13	-11.10	-11.10	-11.16
O I 0.8446	<-20.00	-11.62	-11.62	-11.77
H I 0.9229	-13.95	-11.86	-11.86	-11.69
H I 0.9545	-13.80	-11.72	-11.71	-11.75
[S VIII] 0.9914	-11.90	-11.47	-11.33	-11.50
H I 1.0049	-13.62	-11.54	-11.54	-11.24
[N I] 1.0404	<-20.00	-11.50	-11.50	-11.54
He I 1.0830	-14.99	-10.14	-10.14	-10.30
H I 1.0938	-13.40	-11.33	-11.33	-11.27
O I 1.1287	<-20.00	-11.75	-11.75	-11.92
He II 1.1626	-13.38	-12.09	-12.07	-12.02
He I + [S IX] 1.252	-11.92	-12.36	-11.78	-11.74
H I 1.2818	-13.12	-11.07	-11.07	-11.23
P VII 1.3745	-13.42	-11.50	-11.50	-11.67
[Si X] 1.4300	-11.94	-16.21	-11.94	-11.75
H I 1.6109	-14.80	-12.66	-12.66	-12.71
H I 1.6407	-14.69	-12.57	-12.57	-12.60
H I 1.6806	-14.57	-12.47	-12.47	-12.28
P VIII 1.7393	-12.46	-12.35	-12.10	-12.04
H I 1.7362	-14.46	-12.36	-12.36	-12.04
H I 1.8174	-14.32	-12.23	-12.23	-11.99
H I 1.8751	-12.85	-10.76	-10.76	-10.81
H I 1.9445	-14.16	-12.08	-12.08	-12.10
[Si VI] 1.9624	-14.50	-10.98	-10.98	-11.34
[Al IX] 2.0444	-11.96	-14.48	-11.96	-12.07
He I 2.0581	-19.04	-12.17	-12.17	-12.07
H I 2.1655	-13.98	-11.91	-11.91	-11.97
He II 2.1884	-14.25	-12.97	-12.95	-12.73
[Ca VIII] 2.3211	-12.71	-14.47	-12.70	-12.38
[Si VII] 2.4801	-12.59	-11.27	-11.25	-11.19
[Al V] 2.9045	-17.24	-11.84	-11.84	-11.95
[Mg VIII] 3.0276	-11.15	-13.02	-11.14	-11.11
[Ca IV] 3.2061	-18.70	-12.41	-12.41	-12.31
He II 3.0908	-13.65	-12.34	-12.32	-12.07
[Al VI] 3.6593	-14.28	-12.02	-12.02	-11.88
Al VIII 3.6972	-12.49	-13.72	-12.47	-12.49
H I 3.7395	-14.45	-12.37	-12.37	-12.34
[Si IX] 3.9282	-11.46	-14.96	-11.46	-11.67
H I 4.0511	-13.54	-11.50	-11.49	-11.60

NOTE—

<sup>†</sup> LD/HD = low/high density.

erally lies in the range of 10% to 50% (e.g., [Vanlandingham et al. 2005](#); [Helton et al. 2010](#); [Habtie et al. 2024](#)) depending on several factors including (a) uncertainties in the dereddening value which is wavelength dependent (it is as large as 20% near  $0.7 \mu\text{m}$ , for an error of 0.1 in the  $E_{B-V}$  value), (b) the actual measurement of the line fluxes, (c) the process of removing the H lines from the standard A0V star spectrum (the H lines are numerous, consisting of lines from the Paschen, Brackett, Pfund and Humphreys series), and (d) blending of lines which is a major source of uncertainty in many cases. Given these factors, we consider  $\sigma = 35\%$  for the present study (25% for each line measurement and hence 35% for each line ratio relative to Paschen- $\beta$   $1.2818 \mu\text{m}$ ; the error being added in quadrature while ratioing).

In our analysis the total number of lines is 39, the number of free parameters = 16 and hence the degrees of freedom are 23. We thus get a  $\chi^2 = 59.8$  and a reduced  $\chi_{\text{red}}^2 = 2.6$ . A major part of the  $\chi^2$  value comes from 2 lines, the [O II]  $0.7320, 30 \mu\text{m}$  line ( $\chi^2 = 7.7$ ) and from the [Si VI]  $1.96 \mu\text{m}$  line ( $\chi^2 = 12.8$ ). If these two lines are omitted,  $\chi_{\text{red}}^2 \approx 1.87$ . This is acceptable especially since the assumption of a cylindrical geometry is a significant simplification (e.g., [Pandey et al. 2022](#); [Habtie et al. 2024](#)).

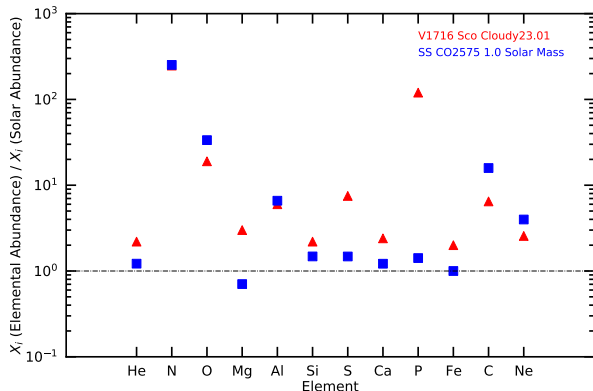


**Figure 5.** The observed abundances (red triangles) derived from the Cloudy photoionization model (assuming a cylindrical geometry) versus model abundance values obtained from tabulated mass fractions (blue squares, [Starrfield et al. 2020](#)) for a  $1.0 M_{\odot}$  CO nova with 25-75% mixing (see Section 4.2 for further details). Solar abundance values are taken from [Grevesse et al. \(2010\)](#). The dashed line across the plot represents solar abundances. The blue square for Fe is set to the solar abundance value as the temperatures reached in the model TNRs are insufficient to produce Fe. The TNR event itself removes the original abundance heritage of the material accreted onto the WD surface by explosive nucleosynthesis reactions ([Starrfield et al. 2020, 2024](#)).

#### 4.2. Abundances Estimates and WD Ejecta Mixing

A comparison of the observed line intensities with the co-added CLOUDY line intensities (the fluxes of high and low density components are co-added) is presented in Figure 4. Considering that a variety of lines are seen (recombination lines, lines from neutral species, lines from highly ionized atoms, Ly $\beta$  fluoresced lines), a reasonably good reproduction of line strengths is seen in Figure 4. H is depleted from nuclear burning in the TNR. We find (Figure 5) that the observationally derived abundances of He, Ne, C, O, Fe, Al, Si, S and Ca are mildly to moderately above solar. The abundances (by mass) with respect to the Sun ([Grevesse et al. 2010](#)) are He = 2.20, C = 6.47, O = 18.99, Ne = 2.56, Mg = 3.00, Al = 6.00, Si = 2.20, S = 7.50, Ca = 2.42, Fe = 2.00, N = 248.00 and P = 120.0. Notably, phosphorus and nitrogen are highly overabundant. However, this is consistent with the predictions of [Starrfield et al. \(2020, 2024\)](#) wherein P is predicted to be 100 or more times overabundant (compared to solar) for massive ONe or CO WDs. For example, for a  $1.25 M_{\odot}$  CO WD with 25-75% mixing the value of P is  $\sim 100$ . The P overabundance may be suggesting that V1716 Sco harbors a massive WD ( $\gtrsim 1.0 M_{\odot}$ ) which is consistent with its short  $t_2$ , (see Section 2.1).

We have compared the derived abundances with those expected in the nucleosynthesis models of [Starrfield et al. \(2020\)](#) as illustrated in Figure 5. This figure compares the observed CLOUDY deduced yields in V1716 Sco with one of the [Starrfield et al. \(2020\)](#) models of an  $1.0 M_{\odot}$  WD with a CO core with 25-75% mixing. A mixing ratio of 25-75% means that the material that undergoes a TNR has a composition of 25% of the outer layers of the underlying WD mixed with 75% of the accreted envelope during the to thermonuclear runaway. The agreement is reasonable for many of the elements.

It is not known whether V1716 Sco contains a WD of the CO or ONe type. The mass of the WD is also not known. However the Fe II classification of the nova ([Walter & Pearce 2023](#)) strongly suggests a CO type. Figure 6 shows a comparison of different models of [Starrfield et al. \(2020, 2024\)](#) for both CO and ONe novae with different WD masses and mixing fractions. For each of the CO and ONe classes, there are six Starrfield models shown with WD masses of 0.6, 0.8, 1.0, 1.15, 1.25 and  $1.35 M_{\odot}$  respectively. For each WD mass, two mixing fractions are considered that of 25-75% and 50-50%. Thus there are a total of twenty-four [Starrfield et al. \(2020, 2024\)](#) models.

[Kelly et al. \(2013\)](#) investigated whether or not observed ONe nova abundances can be used to constrain the degree of mixing that occurs between the outer layers of the underlying WD and the accreted envelope prior to TNR. Any abundance used for this purpose, was referred to as a mixing meter. Comparison of mixing meters with observations allowed for an estimate of the mixing fractions in individual

novae. They found a fraction of 25% or smaller for the mixing between WD matter and the accreted envelope in almost all cases (ONe models). Therefore, Kelly et al. (2013) concluded that the observations support a mixing fraction that is much smaller than 50%, which has usually been used in the literature.

In Figure 6, the meter used is the quantity  $S$  defined as

$$S = \frac{1}{N} \sum_{i=1}^n \left( \frac{x_{\text{obs}}(i)}{x_{\odot}} - \frac{x_{\text{model}}(i)}{x_{\odot}} \right)^2 \quad (3)$$

where the summation is over  $N$  ( $= 11$ ), the number of elements with derived CLOUDY abundances whose mass fractions are compared to those derived for the ejecta for various WD mass in the TNR models of Starrfield et al. (2020, 2024). On the X-axis, each tick label (e.g., CO\_2575) gives the type of the WD (CO or ONe) and the mixing fraction (e.g., 25-75%).

Comparing the CO\_5050 and CO\_2575 values in Figure 6, it is clear that the latter set has much smaller scatter and smaller  $S$  values strongly suggesting that a 25-75% mixing fraction is certainly favored over a 50-50% mixing for V1716 Sco. Further, inter-comparison between the SS ONe and CO models, shows that the observed abundances in V1716 Sco match the CO novae better. A similar conclusion is reached comparing to models by José et al. (2020). This suggests that V1716 Sco is a CO nova, an inference that is consistent with the CO classification proposed in Section 2.1, based on the Fe II spectral classification. Absence of neon lines in the spectra at day 133 also suggests that the binary contains a CO WD, although late-time observations when the source enters a nebular phase combined with detailed abundance modeling may be necessary to confirm the latter assertion (e.g., see the cautionary note in Schwarz et al. 2007) as [Ne V] 3550/3426 Å was detected by Swift near the onset of the SSS phase (Page & Kuin 2023).

As a check for the sensitivity of the results of Figure 6 to errors in the observed flux, we ran an additional two sets of computations with the abundances of all the elements under consideration uniformly increased (or decreased) by  $\pm 20\%$  with respect to H. No significant changes are seen to the results presented in Figure 6.

#### 4.3. Ejecta Mass

The mass ( $M_{\text{shell}}$ ) in a cylindrical volume of height  $h$  can be calculated in units of  $M_{\odot}$  from the parameters presented in Table 1 by the expression:

$$M_{\text{shell}} = \pi m_p (r_{\text{out}}^2 - r_{\text{in}}^2) h (f_{\text{HD}} n_{\text{HD}} + f_{\text{LD}} n_{\text{LD}}) \sum (1 + A_i) \quad (4)$$

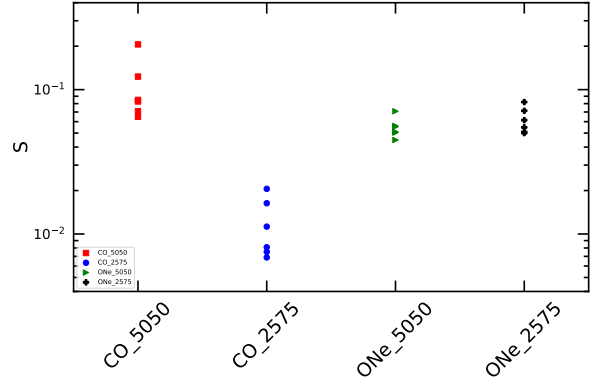


**Figure 6.** Comparison of TNR mixing values to derived abundances in V1716 Sco. Each tick label on the X-axis (e.g., CO\_2575) gives the model values taken from Starrfield et al. (2020, 2024), the type of the WD (CO or ONe) and the mixing fraction (e.g., 25-75%). The multiple points along the Y axis for each tick label correspond to the  $S$  values for the different 6 WD masses (0.6, 0.8, 1.0, 1.15, 1.25, and 1.35  $M_{\odot}$ ) considered in the latter references.  $S$  is essentially a meter to broadly measure how well the observed abundances in V1716 Sco match with nucleosynthesis models (see Section 4.2). A small value of  $S$  implies a good agreement.

where  $f_{\text{HD}}$ ,  $n_{\text{HD}}$ ,  $f_{\text{LD}}$ ,  $n_{\text{LD}}$  are the filling factors and H densities for the high (“clumps”) and low density (“diffuse”) components (abbreviated as HD and LD respectively) given in Table 1,  $m_p$  is the proton mass, and the summation is over the fractional mass of the elements in the shell with respect to hydrogen (using the fraction-by-numbers data in Table 1; other elements not listed in Table 1 are assumed to have solar values). We obtain a mass of  $\simeq 4.19 \times 10^{-4} M_{\odot}$ , (adopting average values of  $n_{\text{HD}}$  and  $n_{\text{LD}}$  assuming  $n(r) = n(r_{\text{in}}) \times r^{-3}$  where  $\sim 88\%$  is in the HD component and  $\sim 12\%$  is in the LD component). This ejected mass estimate is greater than those predicted from TNR models. However, this is a well known tension that has plagued studies of the nova phenomena for decades (e.g., Starrfield 1999; Woodward & Starrfield 2011). The underlying cause for this discrepancy is not understood.

## 5. DISCUSSION

### 5.1. Interpretation of Line Profiles and CLOUDY

There is a clear difference between the shape of the line profiles of the H and He lines, both of which arise from the dense component, and the coronal lines (with ionization potentials of the lower ionization state  $\gtrsim 225$  eV), which mostly arise from the low density component (Table 2). This is illustrated in Figure 7.

H and He lines are broad with a castellated peak emission profile, whereas the infrared coronal lines exhibit distinct double-peaked structures with a deep dip between the

peaks (a notched saddle profile) centered near  $\simeq 0 \text{ km s}^{-1}$ . The lines showing this structure are listed in Table 5 along with the peak-to-peak separation. The highest velocity, common H I recombination line components (Figure 7d) at  $\pm 950 \text{ km s}^{-1}$  are coincident with the double peak profiles seen in neutral oxygen, while the coronal line double peaks are at higher velocities  $\pm 1100 \text{ km s}^{-1}$ . Wings of the coronal lines exhibit even higher velocity substructures in their profiles. The FWHM of the [Mg VIII] profile (Figure 7c) is  $\simeq 3400 \text{ km s}^{-1}$ .

The velocity structures and FWHM suggest that the lines arise from different regions within the ejecta. This is expected because the forbidden coronal lines will be collisionally de-excited in a region that is denser than the critical density of the line (Woodward et al. 2021; Kumar et al. 2022). What is puzzling is that the O I 0.8446 and 1.1287  $\mu\text{m}$  line profiles (excitation potential 12.03 eV, Keenan & Hynes 1950; Bhatia & Kastner 1995) also show a similar profile (albeit somewhat narrower in peak-to-peak separation) as the coronal lines. Modeling indicates (Table 2) oxygen lines also arise within denser regions of the ejecta.

A significant part of the strength of both the 0.8446 and 1.1287  $\mu\text{m}$  lines is from Lyman- $\beta$  fluorescence. So it is consistent that the sites of O I and H emission are co-spatial (Figure 7a) ensuring an adequate input of Ly- $\beta$  photons from the recombination cascade process in hydrogen. If the H emitting region is optically thick, Ly- $\beta$  photons may even get trapped. Thus the necessary sources of Ly- $\beta$  photons are available for fluorescing the O I lines. However, the O I lines show a considerably smaller expansion velocity (FWHM  $\simeq 1350 \text{ km s}^{-1}$ ) than the other coronal lines (FWHM  $\gtrsim 3000 \text{ km s}^{-1}$ ) strongly suggesting that they originate from different regions despite sharing the same double-peaked profile shape.

Likely the V1716 Sco ejecta nebula is not spherically symmetric, but bipolar in morphology. Bipolar morphologies are directly detected in several novae, such as V1280 Sco (Chesneau et al. 2012; Pandey et al. 2022), RS Oph (Bode et al. 2007), V959 Mon (Healy et al. 2017, and references therein) and V445 Pup (Woudt et al. 2009; Nyamai et al. 2021), by using high spatial resolution imaging techniques and interferometry; hence this geometry is common (and why Cloudy models in Section 4.1 explore cylindrical geometries).

In V1716 Sco, denser regions in the asymmetrical ejecta could be the site of the O I 0.8446/1.1287  $\mu\text{m}$  lines and the O I double-peaked profiles could arise from the receding and approaching parts of these lobes. The strong shock created by the ejecta colliding with dense globules, or denser toroidal material within the ejecta could likely have given rise to the  $\gamma$ -rays seen during the outburst. The geometric scenario for the  $\gamma$ -ray generation proposed here would then be similar to that proposed for the  $\gamma$ -ray nova V959 Mon (Chomiuk et al.

2014). In comparison to the O I lines, the coronal lines with a higher velocity (Table 5), could originate from the bipolar lobes which are expected to be more diffuse and also to have a higher velocity compared to the material in a constricting denser torus. Some of the coronal lines with high critical densities in the range of  $10^8$  to  $10^9 \text{ cm}^{-3}$ , like the [Si VI] 1.96 and [Si VII] 2.48  $\mu\text{m}$  lines for gas temperatures in excess of  $10^5 \text{ K}$ , (Evans et al. 2023) could come from both the torus and bipolar lobes. Hence their line profiles are expected to be as evident in Figure 7.

The [N I] 0.5755  $\mu\text{m}$  and 1.04  $\mu\text{m}$  lines, together with the [O I] 0.6300, 0.6364  $\mu\text{m}$  doublet, are among the first forbidden lines to appear in the spectra of novae (particularly the Fe II novae) and they remain present even after high ionization lines appear in the spectra (Williams et al. 1994; Aydi et al. 2024). The [N I] 1.04  $\mu\text{m}$  line is seen here and inspection of optical spectra from the ARAS database<sup>2</sup> shows that [O I] 0.6300, 0.6364  $\mu\text{m}$  lines were present before and during the current observations on day 133. Based on several characteristics of the [O I] emission, Williams et al. (1994) has convincingly argued that dense globules must exist in the ejecta and that the [O I] emission comes from within these globules (these globules are likely sites for dust formation too). Just like the [O I] lines, it would appear reasonable to expect that neutral [N I] 1.04  $\mu\text{m}$  emission also originates from material in the dense globules, where nitrogen atoms can remain shielded and neutral. This is supported by the data in Table 2 which show that [N I] emission arises from the dense component and is absent in the diffuse component.

However, the line profiles (Figure 7) alternatively could be interpreted as being consistent with a single ejecta component (non-spherical, axisymmetric, and inhomogeneous) with just a density gradient imposed by the expansion velocity law. In this picture the higher velocity regions would inevitably be the ones with the lowest density, explaining the broader width and larger peak separation of the IR coronal lines. Conversely in the lower (inner, for an explosive expansion law) velocity regions, recombination occurs, and Ly- $\beta$  can be sufficiently optically thick to pump the observed O I transition.

## 5.2. Observed coronal lines not replicated by CLOUDY

There are two emission lines at  $\sim 1.55$  and  $\sim 2.09 \mu\text{m}$  which are often seen during the coronal stage in many novae, for example V1974 Cyg (Wagner & Depoy 1996), RS Oph (Banerjee et al. 2009), V1674 Her (Woodward et al. 2021) and V6558 Sgr (Gehrz et al. 2018), whose identification has remained uncertain. These lines are thought to be coronal in nature because they arise during the coronal phase and their broader profile shapes (e.g., FWHM and peak-to-peak separation).

<sup>2</sup> [http://www.astrosurf.com/aras/Aras\\_DataBase/Novae.htm](http://www.astrosurf.com/aras/Aras_DataBase/Novae.htm)

rations) often replicate the coronal line profiles shapes (see Gehrz et al. 2018, for a discussion on the 2.09  $\mu\text{m}$  profile shape) rather than the H or He line profiles shapes and sub-structures (see Figure 7 for example).

The line at  $\sim 1.55 \mu\text{m}$  (labeled ‘u.i.’, see Figure 1) has been thought to be either [Si IX] 1.55995  $\mu\text{m}$  or [Cr XI] 1.5518  $\mu\text{m}$  (Wagner & Depoy 1996). However, our CLOUDY calculations underproduce the [Si IX] 1.55995  $\mu\text{m}$  line by a factor of 23,000, while the observed line center is at 1.5534  $\mu\text{m}$ , displaced by 0.0065  $\mu\text{m}$  from the expected position. It is unlikely that this line is [Si IX]. Similarly the observed fluxes of the [Cr XI] 1.5518 and [Mn XIV] 2.09  $\mu\text{m}$  lines in V1716 Sco cannot be matched by CLOUDY even if both these elements are 1000 times overabundant compared to their solar values. It is thus likely that the [Cr XI] and [Mn XIV] assignments to these lines are incorrect. In our CLOUDY models, the strongest lines between 1.5528 - 1.5601  $\mu\text{m}$  are C IV in the low density component, and blends of He I + HI + C IV in the high density component.

### 5.3. Do CNe Produce Helium Hydride ( $\text{HeH}^+$ ) ?

The spectrum of V1716 Sco consists mainly of atomic and ionic lines. However our final CLOUDY model predicts an observable amount of the helium hydride ion,  $\text{HeH}^+$ , in component B (denser component) at a significant column density of  $10^{12.959} \text{ cm}^{-2}$ . The dominant formation channel for  $\text{HeH}^+$  is  $\text{He}^+ + \text{H} \rightarrow \text{HeH}^+ + h\nu$ . Uncertainties in chemical reaction rate coefficients influence the predicted abundances/column densities of the species involved. We adopted the rate coefficient for this reaction from Zygelman & Dalgarno (1990). There can be 30% uncertainty in the predicted column density due to the uncertainties in the chemical rate coefficients (Zygelman & Dalgarno 1990).

After the Big Bang, in the early Universe’s metal-free and low-density environment, the first molecule to form was  $\text{HeH}^+$ , following radiative association of He atoms with protons.  $\text{HeH}^+$  has recently been discovered toward the planetary nebula NCG 7027 via the rotational transition at 149.1  $\mu\text{m}$  (Güsten et al. 2019).  $\text{HeH}^+$  in NGC 7027 has a column density that is similar to that found here for V1716 Sco. The conditions in planetary nebulae are known to be suitable for the production of potentially detectable  $\text{HeH}^+$  column densities: the hard radiation field from the central hot WD creates overlapping Strömgren spheres (Güsten et al. 2019) where  $\text{HeH}^+$  is predicted to form.

Figure 8 shows that a similar situation exists in V1716 Sco (and may possibly exist in other novae) with a similar overlapping of  $\text{He}^+$  and H zones (the CLOUDY model is a time-independent model, hence these are overlapping Strömgren spheres) having substantial number densities of  $\text{HeH}^+$ . In the near-IR,  $\text{HeH}^+$  has a few ro-vibrational features, e.g., the  $\nu = 1 - 0 \text{ P}(1)$  3.51629  $\mu\text{m}$  line, the  $\text{P}(2)$  3.60776  $\mu\text{m}$

**Table 5.** Lines with double peaked profiles

Line	Peak-to-Peak	Line	Peak-to-Peak
	separation		separation
( $\mu\text{m}$ )	( $\text{km s}^{-1}$ )	( $\mu\text{m}$ )	( $\text{km s}^{-1}$ )
O I 0.8446	1705	[Si X] 1.4300	2350
[S VIII] 0.9914	1970	‘u.i.’ 1.5599	2120
O I 1.1287	1807	[Mg VIII] 3.0276	2070
[S IX] 1.2523	2275	[Si IX] 3.9282	2288

line, and the  $\nu = 1 - 0 \text{ R}(0)$  ro-vibrational line at 3.364  $\mu\text{m}$ . The first two of these lines have been detected in NGC 7027 (Neufeld et al. 2020). The line fluxes of these three lines, based on the CLOUDY number densities, need to be calculated theoretically (which is outside the scope of this work) to know whether they should be detectable. However, close examination of our spectrum of V1716 Sco reveals no significant emission at the wavelength positions of these lines, though the atmospheric transmission in the spectral region covered by these lines is poor.

The study of other CNe with the high sensitivity achievable with the JWST NIRSpec may unambiguously detect the presence of this important hydride, and even its evolution in real time or provide more definitive observational evidence that rebuts the conjecture.

## 6. CONCLUSION

A moderate resolution near-IR spectrum of V1716 Sco during the coronal line phase of evolution obtained 132.8 days post-outburst was modeled by using the photoionization code CLOUDY. Abundances were estimated for H, He, N, O, Si, Al, Mg, S, Ca and P. Except for H, the analyzed elements are over-abundant compared to solar values. The abundances (by mass) with respect to the Sun are He = 2.20, C = 6.47, O = 18.99, Ne = 2.56, Mg = 3.00, Al = 6.00, Si = 2.20, S = 7.50, Ca = 2.42, Fe = 2.00, N = 248.00 and P = 120.0.

It was necessary to consider the ejecta to be composed of two components. One, a dense component from which the bulk of the H, He, OI and N emission arises and second, a less dense component from which most of the coronal lines arise. Some of the coronal lines are found to arise from both components. A cylindrical (non-spherical) geometry for the ejecta in photoionization modeling best reproduces the observed IR line fluxes. The mass of the ejecta, including neutral and ionized gas, is  $\simeq 4.19 \times 10^{-4} M_{\odot}$ .



The Ly- $\beta$  fluoresced O I 0.8446 and 1.1287  $\mu\text{m}$  lines exhibit a prominent double-peaked structure; a profile shape that the O I lines share with several coronal lines.

Finally, the derived abundance yields were compared to various simulations of the TNR event to assess and constrain the level of potential mixing (Starrfield et al. 2020, 2024). Our analysis suggests that in the case of V1716 Sco (which has a CO WD), a fraction of 25% rather than 50% is favored for the mixing between WD matter and the accreted envelope before the outburst. This is similar to the 25% mixing fraction that is favored in O Ne novae (Kelly et al. 2013) and elsewhere.

### Acknowledgements

The authors wish to acknowledge the referee for their insight and constructive critiques that improved the manuscript. The authors also are deeply indebted to Dr. D. P. K. Banerjee for his in depth discussion that paved the way for the analysis and interpretation of these data. We also acknowledge with thanks the variable star observations from the *AAVSO International Database* contributed by observers worldwide and used in this research. The optical spectroscopic data from ARAS site (*Astronomical Ring for Amateur Spectroscopy*) was helpful in our analysis. We are most grateful to Paul Kuin for exploring the availability of Swift UV spectra contemporaneous with the near-IR observations. GS acknowledges a WOS-A grant from the Department of Science and Technology (SR/WOS-A/PM- 2/2021). KLP acknowledges funding from the UK Space Agency. We thank John Rayner, Director IRTF, for Director’s Discretionary Time (2023B988) who made scheduling of this program possible and the IRTF telescope operator for assisting CEW with the observations. The Infrared Telescope Facility, is operated by the University of Hawaii under contract 80HQTR19D0030 with the National Aeronautics and Space Administration. SS acknowledges partial support from a NASA Emerging Worlds grant to ASU (80NSSC22K0361) as well as support from his ASU Regents’ Professorship. The x-ray data underlying this paper are available in the Swift archive at [https://www.swift.ac.uk/swift\\_live/](https://www.swift.ac.uk/swift_live/) and the HEASARC Browse archive at <https://heasarc.gsfc.nasa.gov/cgi-bin/W3Browse/w3browse.pl>. This work has made use of data from the European Space Agency (ESA) mission *Gaia* (<https://www.cosmos.esa.int/gaia>), processed by the *Gaia* Data Processing and Analysis Consortium (DPAC, <https://www.cosmos.esa.int/web/gaia/dpac/consortium>). Funding for the DPAC has been provided by national institutions, in particular the institutions participating in the *Gaia* Multilateral Agreement.

*Facilities:* AAVSO, IRTF (SpeX), Swift, Gaia, DECaps

*Software:* Astro Data Lab (Nikutta et al. 2020), Astropy (Astropy Collaboration et al. 2018), CLOUDY (Ferland et al.

1998; Chatzikos et al. 2023), Spextool (Cushing et al. 2004), HEASOFT/XSPEC (Arnaud 1996).

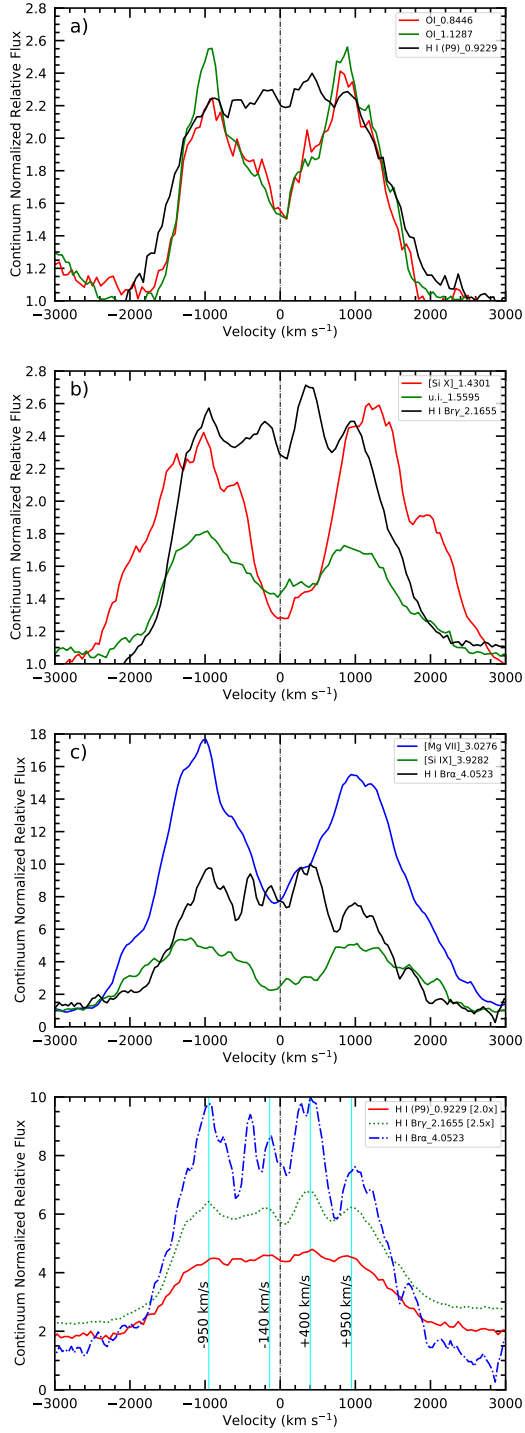


**Figure 7.** Emission line velocity profiles of V1716 Sco on day +132.8. Each emission line is normalized to the average adjacent continuum and scaled (as indicated in the inset). The vertical black dashed line in each panel is 0 km s<sup>-1</sup>, and the ‘u.i.’ label indicates unidentified line. a) Lines of neutral oxygen O I 0.8446 and 1.1287 μm versus H I (P9) 0.9229 μm. b) Coronal lines of [Si IX] versus H I Brγ in the SpeX SXD mode. c) Coronal lines [Mg VII] and [Si IX] in the thermal IR (λ ≳ 3.0 μm) versus H I Brα in the SpeX LXD\_short mode. The FWHM of the [Mg VIII] profile is ≃ 3400 km s<sup>-1</sup>. d) Common velocity components present in the H I recombination line profiles (vertical black arrows).

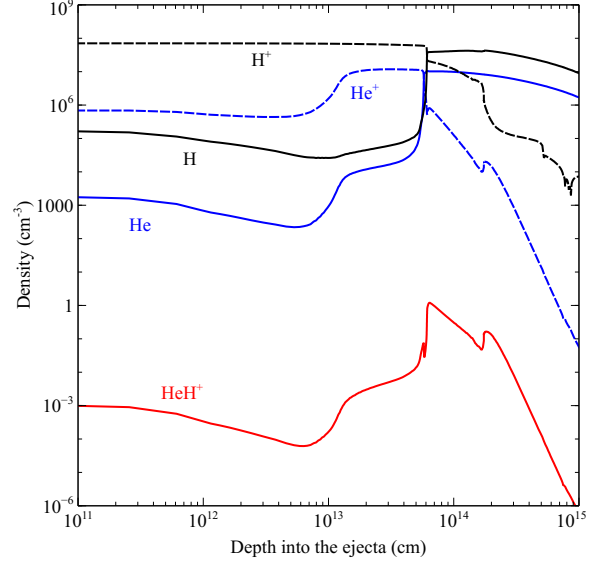


**Figure 8.** CLOUDY derived number densities (cm<sup>-3</sup>) of HeH<sup>+</sup> (red) and that of He (blue) and H<sup>+</sup> (black) as a function of depth into the nova ejecta (cm) in V1716 Sco (+133 d). The ionization front is near ≃ 6 × 10<sup>13</sup> cm.



## REFERENCES

- Anupama, G. C., & Kamath, U. S. 2012, *Bulletin of the Astronomical Society of India*, 40, 161
- Arnaud, K. A. 1996, in *Astronomical Society of the Pacific Conference Series*, Vol. 101, *Astronomical Data Analysis Software and Systems V*, ed. G. H. Jacoby & J. Barnes, 17
- Astropy Collaboration, Price-Whelan, A. M., Sipőcz, B. M., et al. 2018, *AJ*, 156, 123, doi: [10.3847/1538-3881/aabc4f](https://doi.org/10.3847/1538-3881/aabc4f)
- Aydi, E., Chomiuk, L., Strader, J., et al. 2024, *MNRAS*, 527, 9303, doi: [10.1093/mnras/stad3342](https://doi.org/10.1093/mnras/stad3342)
- Bailer-Jones, C. A. L., Rybizki, J., Fouesneau, M., Demleitner, M., & Andrae, R. 2021, *AJ*, 161, 147, doi: [10.3847/1538-3881/abd806](https://doi.org/10.3847/1538-3881/abd806)
- Banerjee, D. P. K., Das, R. K., & Ashok, N. M. 2009, *MNRAS*, 399, 357, doi: [10.1111/j.1365-2966.2009.15279.x](https://doi.org/10.1111/j.1365-2966.2009.15279.x)
- Banerjee, D. P. K., Srivastava, M. K., Ashok, N. M., & Venkataraman, V. 2016, *MNRAS*, 455, L109, doi: [10.1093/mnras/slv163](https://doi.org/10.1093/mnras/slv163)
- Benjamin, R. A., & Dinerstein, H. L. 1990, *AJ*, 100, 1588, doi: [10.1086/115619](https://doi.org/10.1086/115619)
- Bhatia, A. K., & Kastner, S. O. 1995, *ApJS*, 96, 325, doi: [10.1086/192121](https://doi.org/10.1086/192121)
- Bode, M. F., & Evans, A. 2012, *Classical Novae*
- Bode, M. F., Harman, D. J., O'Brien, T. J., et al. 2007, *ApJL*, 665, L63, doi: [10.1086/520929](https://doi.org/10.1086/520929)
- Cardelli, J. A., Clayton, G. C., & Mathis, J. S. 1989, *ApJ*, 345, 245, doi: [10.1086/167900](https://doi.org/10.1086/167900)
- Celedón, L., Schmidtbreick, L., Tappert, C., & Selman, F. 2024, *A&A*, 681, A106, doi: [10.1051/0004-6361/202347215](https://doi.org/10.1051/0004-6361/202347215)
- Chatzikos, M., Bianchi, S., Camilloni, F., et al. 2023, *RMxAA*, 59, 327, doi: [10.22201/ia.01851101p.2023.59.02.12](https://doi.org/10.22201/ia.01851101p.2023.59.02.12)
- Chesneau, O., Lagadec, E., Otulakowska-Hypka, M., et al. 2012, *A&A*, 545, A63, doi: [10.1051/0004-6361/201219825](https://doi.org/10.1051/0004-6361/201219825)
- Cheung, C. C., Jean, P., Shore, S. N., Grove, J. E., & Leising, M. 2015, in *International Cosmic Ray Conference*, Vol. 34, 34th International Cosmic Ray Conference (ICRC2015), 880, doi: [10.22323/1.236.0880](https://doi.org/10.22323/1.236.0880)
- Cheung, C. C. T., Jean, P., Stawarz, L., & Shore, S. N. 2018, in 42nd COSPAR Scientific Assembly, Vol. 42, E1.7–37–18
- Chomiuk, L., Metzger, B. D., & Shen, K. J. 2021, *ARA&A*, 59, 391, doi: [10.1146/annurev-astro-112420-114502](https://doi.org/10.1146/annurev-astro-112420-114502)
- Chomiuk, L., Linford, J. D., Yang, J., et al. 2014, *Nature*, 514, 339, doi: [10.1038/nature13773](https://doi.org/10.1038/nature13773)
- Cushing, M. C., Vacca, W. D., & Rayner, J. T. 2004, *PASP*, 116, 362, doi: [10.1086/382907](https://doi.org/10.1086/382907)
- Das, R. K., Banerjee, D. P. K., & Ashok, N. M. 2009, *MNRAS*, 398, 375, doi: [10.1111/j.1365-2966.2009.15141.x](https://doi.org/10.1111/j.1365-2966.2009.15141.x)
- De, K., Kasliwal, M. M., Hankins, M. J., et al. 2021, *ApJ*, 912, 19, doi: [10.3847/1538-4357/abeb75](https://doi.org/10.3847/1538-4357/abeb75)
- Dere, K. P. 2007, *A&A*, 466, 771, doi: [10.1051/0004-6361:20066728](https://doi.org/10.1051/0004-6361:20066728)
- Evans, A., Banerjee, D. P. K., Woodward, C. E., et al. 2023, *MNRAS*, 522, 4841, doi: [10.1093/mnras/stad1209](https://doi.org/10.1093/mnras/stad1209)
- Evans, A., & Gehrz, R. D. 2012, *Bulletin of the Astronomical Society of India*, 40, 213, doi: [10.48550/arXiv.1209.3193](https://doi.org/10.48550/arXiv.1209.3193)
- Ferland, G. J., Korista, K. T., Verner, D. A., et al. 1998, *PASP*, 110, 761, doi: [10.1086/316190](https://doi.org/10.1086/316190)
- Gaia Collaboration, Vallenari, A., Brown, A. G. A., et al. 2023, *A&A*, 674, A1, doi: [10.1051/0004-6361/202243940](https://doi.org/10.1051/0004-6361/202243940)
- Gehrels, N., Chincarini, G., Giommi, P., et al. 2004, *ApJ*, 611, 1005, doi: [10.1086/422091](https://doi.org/10.1086/422091)
- Gehrz, R. D., Truran, J. W., Williams, R. E., & Starrfield, S. 1998, *PASP*, 110, 3, doi: [10.1086/316107](https://doi.org/10.1086/316107)
- Gehrz, R. D., Evans, A., Woodward, C. E., et al. 2018, *ApJ*, 858, 78, doi: [10.3847/1538-4357/aaba81](https://doi.org/10.3847/1538-4357/aaba81)
- Glasner, S. A., Livne, E., & Truran, J. W. 2012, *MNRAS*, 427, 2411, doi: [10.1111/j.1365-2966.2012.22103.x](https://doi.org/10.1111/j.1365-2966.2012.22103.x)
- Greenhouse, M. A., Grasdalen, G. L., Woodward, C. E., et al. 1990, *ApJ*, 352, 307, doi: [10.1086/168537](https://doi.org/10.1086/168537)
- Grevesse, N., Asplund, M., Sauval, A. J., & Scott, P. 2010, *Ap&SS*, 328, 179, doi: [10.1007/s10509-010-0288-z](https://doi.org/10.1007/s10509-010-0288-z)
- Güsten, R., Wiesemeyer, H., Neufeld, D., et al. 2019, *Nature*, 568, 357, doi: [10.1038/s41586-019-1090-x](https://doi.org/10.1038/s41586-019-1090-x)
- Habtie, G. R., Das, R., Pandey, R., Ashok, N. M., & Dubovsky, P. A. 2024, *MNRAS*, 527, 1405, doi: [10.1093/mnras/stad3295](https://doi.org/10.1093/mnras/stad3295)
- Healy, F., O'Brien, T. J., Beswick, R., Avison, A., & Argo, M. K. 2017, *MNRAS*, 469, 3976, doi: [10.1093/mnras/stx1087](https://doi.org/10.1093/mnras/stx1087)
- Helton, L. A., Woodward, C. E., Walter, F. M., et al. 2010, *AJ*, 140, 1347, doi: [10.1088/0004-6256/140/5/1347](https://doi.org/10.1088/0004-6256/140/5/1347)
- Izzo, L., Della Valle, M., Woodward, C. E., et al. 2023, *The Astronomer's Telegram*, 16007, 1
- José, J., Shore, S. N., & Casanova, J. 2020, *A&A*, 634, A5, doi: [10.1051/0004-6361/201936893](https://doi.org/10.1051/0004-6361/201936893)
- Keenan, P. C., & Hynek, J. A. 1950, *ApJ*, 111, 1, doi: [10.1086/145231](https://doi.org/10.1086/145231)
- Kelly, K. J., Iliadis, C., Downen, L., José, J., & Champagne, A. 2013, *ApJ*, 777, 130, doi: [10.1088/0004-637X/777/2/130](https://doi.org/10.1088/0004-637X/777/2/130)
- Kemp, A. J., Karakas, A. I., Casey, A. R., et al. 2022, *ApJL*, 933, L30, doi: [10.3847/2041-8213/ac7c72](https://doi.org/10.3847/2041-8213/ac7c72)
- Kumar, V., Srivastava, M. K., Banerjee, D. P. K., et al. 2022, *MNRAS*, 510, 4265, doi: [10.1093/mnras/stab3772](https://doi.org/10.1093/mnras/stab3772)
- Marshall, D. J., Robin, A. C., Reylé, C., Schultheis, M., & Picaud, S. 2006, *A&A*, 453, 635, doi: [10.1051/0004-6361:20053842](https://doi.org/10.1051/0004-6361:20053842)
- Molaro, P., Izzo, L., D'Odorico, V., et al. 2022, *MNRAS*, 509, 3258, doi: [10.1093/mnras/stab3106](https://doi.org/10.1093/mnras/stab3106)
- Molaro, P., Izzo, L., Selvelli, P., et al. 2023, *MNRAS*, 518, 2614, doi: [10.1093/mnras/stac2708](https://doi.org/10.1093/mnras/stac2708)

- Neufeld, D. A., Goto, M., Geballe, T. R., et al. 2020, *ApJ*, 894, 37, doi: [10.3847/1538-4357/ab7191](https://doi.org/10.3847/1538-4357/ab7191)
- Nikutta, R., Fitzpatrick, M., Scott, A., & Weaver, B. A. 2020, *Astronomy and Computing*, 33, 100411, doi: [10.1016/j.ascom.2020.100411](https://doi.org/10.1016/j.ascom.2020.100411)
- Nyamai, M. M., Chomiuk, L., Ribeiro, V. A. R. M., et al. 2021, *MNRAS*, 501, 1394, doi: [10.1093/mnras/staa3712](https://doi.org/10.1093/mnras/staa3712)
- Page, K. L., & Kuin, N. P. M. 2023, *The Astronomer's Telegram*, 16069, 1
- Pandey, R., Das, R., Shaw, G., & Mondal, S. 2022, *ApJ*, 925, 187, doi: [10.3847/1538-4357/ac36dc](https://doi.org/10.3847/1538-4357/ac36dc)
- Politano, M., Starrfield, S., Truran, J. W., Weiss, A., & Sparks, W. M. 1995, *ApJ*, 448, 807, doi: [10.1086/176009](https://doi.org/10.1086/176009)
- Pontefract, M., & Rawlings, J. M. C. 2004, *MNRAS*, 347, 1294, doi: [10.1111/j.1365-2966.2004.07330.x](https://doi.org/10.1111/j.1365-2966.2004.07330.x)
- Raj, A., Ashok, N. M., Rudy, R. J., et al. 2015, *AJ*, 149, 136, doi: [10.1088/0004-6256/149/4/136](https://doi.org/10.1088/0004-6256/149/4/136)
- Rayner, J. T., Toomey, D. W., Onaka, P. M., et al. 2003, *PASP*, 115, 362, doi: [10.1086/367745](https://doi.org/10.1086/367745)
- Robinson, G. J., Reay, N. K., & Atherton, P. D. 1982, *MNRAS*, 199, 649, doi: [10.1093/mnras/199.3.649](https://doi.org/10.1093/mnras/199.3.649)
- Rudy, R. J., Dimpfl, W. L., Lynch, D. K., et al. 2003, *ApJ*, 596, 1229, doi: [10.1086/378083](https://doi.org/10.1086/378083)
- Saydjari, A. K., Schlafly, E. F., Lang, D., et al. 2023, *ApJS*, 264, 28, doi: [10.3847/1538-4365/aca594](https://doi.org/10.3847/1538-4365/aca594)
- Schwarz, G. J., Woodward, C. E., Bode, M. F., et al. 2007, *AJ*, 134, 516, doi: [10.1086/519240](https://doi.org/10.1086/519240)
- Shore, S., Charbonnel, S., Le Du, P., et al. 2023a, *The Astronomer's Telegram*, 16004, 1
- . 2023b, *The Astronomer's Telegram*, 16006, 1
- . 2023c, *The Astronomer's Telegram*, 16036, 1
- Sokolovsky, K., Aydi, E., Chomiuk, L., et al. 2023, *The Astronomer's Telegram*, 16018, 1
- Srivastava, M. K., Banerjee, D. P. K., Ashok, N. M., et al. 2016, *MNRAS*, 462, 2074, doi: [10.1093/mnras/stw1807](https://doi.org/10.1093/mnras/stw1807)
- Starrfield, S. 1999, *PhR*, 311, 371, doi: [10.1016/S0370-1573\(98\)00116-1](https://doi.org/10.1016/S0370-1573(98)00116-1)
- Starrfield, S., Bose, M., Iliadis, C., et al. 2020, *ApJ*, 895, 70, doi: [10.3847/1538-4357/ab8d23](https://doi.org/10.3847/1538-4357/ab8d23)
- . 2024, *ApJ*, 962, 191, doi: [10.3847/1538-4357/ad1836](https://doi.org/10.3847/1538-4357/ad1836)
- Toraskar, J., Mac Low, M.-M., Shara, M. M., & Zurek, D. R. 2013, *ApJ*, 768, 48, doi: [10.1088/0004-637X/768/1/48](https://doi.org/10.1088/0004-637X/768/1/48)
- Vacca, W. D., Cushing, M. C., & Rayner, J. T. 2003, *PASP*, 115, 389, doi: [10.1086/346193](https://doi.org/10.1086/346193)
- van den Bergh, S., & Younger, P. F. 1987, *A&AS*, 70, 125
- Vanlandingham, K. M., Schwarz, G. J., Shore, S. N., Starrfield, S., & Wagner, R. M. 2005, *ApJ*, 624, 914, doi: [10.1086/428895](https://doi.org/10.1086/428895)
- Voronov, G. S. 1997, *Atomic Data and Nuclear Data Tables*, 65, 1, doi: [10.1006/adnd.1997.0732](https://doi.org/10.1006/adnd.1997.0732)
- Wagner, R. M., & Depoy, D. L. 1996, *ApJ*, 467, 860, doi: [10.1086/177659](https://doi.org/10.1086/177659)
- Walter, F. M., & Pearce, A. 2023, *The Astronomer's Telegram*, 16003, 1
- Williams, R. E., Phillips, M. M., & Hamuy, M. 1994, *ApJS*, 90, 297, doi: [10.1086/191864](https://doi.org/10.1086/191864)
- Woodward, C. E., Banerjee, D. P. K., Geballe, T. R., et al. 2021, *ApJL*, 922, L10, doi: [10.3847/2041-8213/ac3518](https://doi.org/10.3847/2041-8213/ac3518)
- Woodward, C. E., Evans, A., & Banerjee, D. K. P. 2023, *The Astronomer's Telegram*, 16222, 1
- Woodward, C. E., & Starrfield, S. 2011, *Canadian Journal of Physics*, 89, 333, doi: [10.1139/p11-010](https://doi.org/10.1139/p11-010)
- Woudt, P. A., Steeghs, D., Karovska, M., et al. 2009, *ApJ*, 706, 738, doi: [10.1088/0004-637X/706/1/738](https://doi.org/10.1088/0004-637X/706/1/738)
- Zygelman, B., & Dalgarno, A. 1990, *ApJ*, 365, 239, doi: [10.1086/169475](https://doi.org/10.1086/169475)